Mechanical characterization of “Scaglia Rossa” stone masonry through experimental and numerical analyses

Mechanical characterization of "Scaglia Rossa" stone masonry through experimental and numerical analyses

Georgios Panagiotis Salachoris[1], Erica Magagnini[1], Francesco Clementi[1,*]

[1]Department of Civil and Building Engineering, and Architecture,
Polytechnic University of Marche,
Via Brecce Bianche n.12, 60131 Ancona, Italy
g.p.salachoris@pm.univpm.it; e.magagnini@staff.univpm.it; francesco.clementi@univpm.it

*Corresponding authors: francesco.clementi@univpm.it ; Tel. +39 071 220 4569

Abstract

This paper outlines the complete characterization of masonry walls composed of "Scaglia Rossa", a typical stone of the Apennine area between the Umbria and Marche Regions in Central Italy. The study focuses the assessment of the mechanical behavior by means of an experimental campaign carried out in the laboratory of the Polytechnic University of Marche, where the samples of "Scaglia Rossa" masonry, obtained from the controlled demolition of three school buildings, were reconstructed with the same techniques of the 1950s-'60s, and then tested in order to identify both the constituent materials, stone and mortar, and the composite masonry.

The experimental tests were prior to a numerical analysis implemented by the adoption of a nonlinear model capturing the cracking behavior. The main mechanical parameters were then calibrated by means of an optimization algorithm of Levenberg-Marquardt, considering a continuous approach with both (i) macro- and (ii) micro-modelling techniques and obtaining resistance parameters not deriving directly from the experimental tests. The comparison between the results obtained from the Levenberg - Marquardt algorithm by changing the parameters of the damage model based on data given by the experimental campaign allowed to confirm the validity of the approach used.

Keywords: Central Italy earthquake, masonry, experimental tests, FE modeling, optimization algorithm, calibration.

1. INTRODUCTION

The scientific community of many different research areas was moved by recent seismic activity all over the World [1,2], moreover in Southern Europe [3–5], that caused such dramatic damages to architectural heritage, not to mention all the deaths and injuries, lead to the need of an exhaustive investigation on the quality of materials and buildings. The features of constructions are, indeed, fundamental to a full comprehension of how the historical building heritage behaves when it is struck by both static and dynamic (such as seismic) actions [6].

Moreover, Italy has been affected by numerous earthquakes down the ages, and some of these events, namely the Friuli (1976), Irpinia (1980), Umbria-Marche (1996-1997), Molise (2002), L'Aquila (2009), Emilia-Romagna (2012), and Central Italy (2016-2017) earthquakes outlined how every restoration project shall be preceded by a meticulous damage assessment.

Each one of the above-mentioned catastrophic events was characterized by a huge number of heavily damaged buildings and collapses, showing how fundamental an adequate assessment preceding any restoration [7] is, since all the damaging appear to have a common ground made by the poor quality of the mechanical characteristics of masonry, together with the lack of connection both between walls and between these and horizontal elements. The masonry's quality, determined by the peculiarities of both mortar and stone, may be seen as a starting point of any diagnosis since the processes of prevention and rehabilitation can be successfully accomplished only if the actual state of the building is certain. Moreover, it appears to be impossible to properly manage a restoration project when neither the state of the art of the construction procedure nor the effectiveness of the repairs is known.

The behavior of the masonry's components, i.e. mortars and stones, becomes thus fundamental since masonry itself is a composite material, usually obtained by joining natural or artificial bricks by means of mortar layers. The high variability of its components, due to numerous factors such as different local construction technologies leads to a not uniquely classifiable inhomogeneous material [8].

Even though stiffness and resistance have a great dispersion for the above-mentioned reason, they could still characterize the masonry material of ancient constructions by means of average values, not only provided by codes or manuals but also from experimental campaigns.

The formulation of models properly reproducing the complex nonlinear mechanical behavior of the masonry is indeed an active research field, since the nonlinear response may be seen as one of the many challenges of structural engineering, as it is triggered by even the lowest deformation levels.

It is widely assessed by current literature that the mechanical behavior of masonry is dominated by the nonlinear phase, characterized by cracks opening, dissipative and brittle behavior with a softening branch, requiring nonlinear anisotropic constitutive laws since its behavior is remarkably different in terms of tension and compression. The adoption of continuous material models appears to be the most natural approach to describe the mechanical behavior of masonry structural elements, hence much focus is currently put on the formulation of nonlinear constitutive relationships for masonry, thus a large number of models is currently available [9–13]. In this framework, a wide variety of continuous 2D and 3D nonlinear models is proposed; these include complex nonlinear mechanisms such as friction-plasticity, cohesion, crushing, damage and others [14–17].

Most of the Italian Regions has shown an intense seismic activity through the centuries, especially in the Apennine area, between Umbria and Marche, where the building heritage is characterized by a rural, i.e. vernacular, masonry. The design is made by roughly cut stones used for the walls and lime-based mortars used for connectivity, leading to a substantial similarity of construction techniques, even though a strong differentiation of the materials is linked to site availability. Starting from the Middle Ages until the first decades of XX century this basic and sustainable construction technique was based on materials obtained from quarries located near the urban centers. They were used to produce masonry sections that varied in the range of 45–60 cm to create manufactures that were usually from one to a maximum of three floors high.

Central Italy, the area under investigation in this paper, was dramatically damaged during World War II and then rebuilt in a fast process, most of the time in absence of adequate funds [18], that led to the

use of the “Scaglia Rossa” stone, a local, easily available rock but rarely used in the past to refurbish the building patrimony. “Scaglia Rossa”, along with cement-based mortars, was commonly used between 1950-60’s in place of bricks, tuff, and centrifuged concrete blocks since these materials were introduced in this area only around 1970’s. Unsurprisingly, the study carried on “Scaglia Rossa” based walls, made by operators lacking experience in managing a basically new material in a non-controlled, almost vernacular process, highlights a wide range of resistance values. This type of masonry was deployed on both civil structures [19] and medium-small schools [20] and was not taken into account by recent literature, focusing on medieval, Renaissance and late classical masonries’ which presented greater damage also due to disintegration [3,21–23], due to the fact that “Scaglia Rossa” did not show any particular damage caused by the seismic crisis of Umbria-Marche in 1997. Conversely, it was dramatically affected by the more recent seismic activity that stroked Central Italy in 2016-2017 (Fig. 1), depicting how a complete characterization of the “Scaglia Rossa” masonry is fundamental to the reconstruction work currently underway in that same area. It is crucial to provide professionals, as previously done on past earthquakes [6], with firstly quantitative and then qualitative indications, filling a void in the current bibliography by developing extensive technical reports on the mechanical characteristics of soils and masonry structures typical of this part of Italy.

This paper focuses on how the understanding of the exact nonlinear and three-dimensional behavior of the “Scaglia Rossa” masonry is crucial to detect all the structural frailties usually triggered by earthquakes. An experimental campaign is preliminarily devised at the “Laboratorio Prove Materiali e Strutture” of the Polytechnic University of Marche (Ancona, Italy), starting from the samples of “Scaglia Rossa” deriving from the demolitions of some structures from San Ginesio, San Severino Marche and Matelica, small towns located in the Apennine area in the province of Macerata (Marche Region, Central Italy). Then, the mechanical parameters are calibrated in order to catch the evolution of the damage at different scales of modelling and to grant a better understanding of the main mechanical parameters involved, by means of an optimization algorithm of Levenberg-Marquardt, considering a continuous approach with both (i) macro- and (ii) micro-modelling techniques [24].

Figure 1 - Damage on "Scaglia Rossa" masonry structures after Central Italy seismic sequence.

The paper is organized as follows. In **Sect. 2** we describe the "Scaglia Rossa" stone from also a geological point of view. **Sect. 3** provides a look at the effects of the Central Italy seismic sequence of 2016-2017 in structures made with "Scaglia Rossa". In **Sect. 4**, the experimental campaign is reported, allowing to evaluate the main mechanical parameters of stone, mortar and masonry's walls. In **Sect. 5**, the numerical simulations and the main results are summarized for both the numerical strategies used. The paper ends by drawing some conclusions (**Sect. 6**).

2. GEOLOGICAL AND STRATIGRAPHIC SETTINGS OF "SCAGLIA ROSSA" FORMATION

"Scaglia Rossa" is common in the Apennine area crossing the Marche and Umbria Regions, even though some traces of its presence are also evident in the Euganean area and in Southern calcareous

Alps. According to the Italian naming convention used to define limestones, “Scaglia” rocks are characterized not only by their color but also by their stepped outline. The “Scaglia Rossa” stone, deriving from the pelagic environment, show a fine – grained silex calcareous lithology; its shades may vary from white, yellow and ash yellow to intense crimson, hence its name would refer to its color, due to the presence of iron oxide (limonite and hematite) in the chalk mass. Lighter shades, form a light yellow to white, may be caused by secondary discoloring.

The “Scaglia Rossa” limestone was deposited from 55 to 90 million years ago during the superior Cretaceous period and partially the lower Eocene, thus its structure usually displays a dense, regular stratification, characterized by layers that may reach a 100m thickness; red silex nodes on the inside are also very common as the limestone is rich in fossils, such as sea urchins, lamellibranch mollusks and remains of sharks. Its microfossils content is basically made by planktonic foraminifera like Globotruncanae, Heterohelix and Rosita Contusa (before the mass extinction of Cretaceous Paleocene), Morzovellae and Planorotaliae (post K-T).

3. THE DAMAGE ON “SCAGLIA ROSSA” STRUCTURES DURING CENTRAL ITALY EARTHQUAKE OF 2016-17

After the II World War, the Apennine area between Marche and Umbria was built with a relatively new, if compared to the past techniques, local stone, easily available, namely “Scaglia Rossa”, which monopolized constructions between 1950-60’s instead of bricks, tuff, and centrifuged concrete blocks which were introduced in this area around 1970’s.

Prior to investigating the mechanical characterization of the “Scaglia Rossa” masonry, it would be proper to pay attention to the damages caused by the Central Italy seismic sequence of 2016-2017 to the structures consisting of this particular limestone, considering detriment is frequently more distinguishable in structures having more than two storeys above ground [19]. These structures are usually isolated and have a minimum of 2 to a maximum of 4 elevations. The roof is generally inclined and made with the same floor slabs.

Seismic activities showed how “Scaglia Rossa” masonry usually had two to three not evenly connected layers across the thickness. Most of the floors are partially cast in place, lacking a clear reinforced concrete slab at the extrados which means that the diaphragm behaviour of the floor is not infinitely rigid. Moreover, the presence of rough and irregular stones, combined with the use of a cement mortar characterised by reduced mechanical properties highlighted a tendency to disintegration in most cases (Fig. 1).

The damages reported clearly shows that, at the end of the seismic sequence, cases of incipient disintegration of the masonry and triggering of out-of-plane mechanisms were rare when compared to the frequent cracks in the panel plane. Even though there are very few "Scaglia Rossa" structures without serious damage, they have had a good overall behaviour because only very few collapses were recorded concerning the initial stock.

Finally, it should be noted that the greatest damage was observed in the presence of seismic amplification due to the stratigraphy (soil-structure interaction) and topography of the construction site under repeated shocks. This leads to assess that the effect of damage accumulation played a significant role in defining the actual damage of some settlements, although the difference in the quality of structural details and masonry is decisive for the seismic response of buildings to a seismic sequence.

4. EXPERIMENTAL CAMPAIGN

The experimental campaign was carried out in the “Laboratorio Prove Materiali e Strutture” of the Polytechnic University of Marche (Ancona, Italy), where the samples of “Scaglia Rossa” masonry, deriving from the controlled demolition of three school buildings, were first reconstructed with the same techniques of the 1950s-‘60s then tested to identify both the constituent materials, stone and mortar, and the composite masonry.

The main results of these tests are reported in the following paragraphs. At first, load-bearing tests were carried out for the “Scaglia Rossa” specimens, to obtain the compressive resistance of the

limestone. Subsequently, four walls were built with a cement mortar mixture with percentages from that time (1950-‘60s). During the construction of the four wall specimens, mortar samples were extracted and then tested by 3-point bending and load-bearing tests (on the two remaining portions), after 28 days of curing. To eliminate the action of different curing times, the mortar tests were conducted on the same day as the tests of the walls.

4.1. “Scaglia rossa” stone mechanical characterization

The compressive strength of “Scaglia Rossa” stone was obtained according to UNI EN 1926:2007 and [7]. The specimens were made by milling Scaglia Rossa stones chosen from the available lot (Figs. 2(a) and (b)). The specimen side is of about 70±5 mm as reported in Table 1, and they all were conditioned to a temperature of 70°C until a constant mass was obtained. Specimens were capped and tested directly between steel plates: blocks’ surfaces were sufficiently flat and parallel. The monotonic tests were performed with the aid of a load-bearing apparatus.

(a) *(b)*

Figure 2 - “Scaglia Rossa” stone (a) and cubic specimens derived from the cut (b).

Six specimens were prepared, with different grades of the colour of “Scaglia Rossa” material, to consider the influence of different geological compositions. All the specimens showed a break with an hourglass like shape. From these tests an average value of $f_{c,s,medium}$=131.26 MPa is observed for the stock; considering the two slightly different compositions of the stones, an average compressive

value equal to 128.74 MPa for the red, and 133.77 MPa for the white stones are advisable, which will be used in subsequent calibrations. All these values are in good agreement with those reported in [25] where a strength range between 109÷140 MPa is reported.

Finally, it is important to stress the fact that, given the small size of the specimens and the impossibility of applying strain gauges, the displacement-force curves are not available.

Table 1 – Stone specimens under compression tests.

N.	Rock Colour	Area (mm^2)	Failure Load (kN)	$f_{c,s}$ (MPa)
Stone spec. n.1	Red	5030.35	605	120.26
Stone spec. n.2	Red	5062.20	640	126.42
Stone spec. n.3	Red	5087.25	710	139.56
Stone spec. n.4	White	5055.21	785	155.28
Stone spec. n.5	White	5041.00	730	144.81
Stone spec. n.6	White	5037.45	510	101.24

4.2. Mortar mechanical characterization

The mechanical characterization of the mortar was carried out according to the UNI EN 1015-11:2019, the regulations of [7] and [11]. For masonry mortar, monotonic three-point bending, and load-bearing tests were performed on the specimens directly obtained during the construction of the walls which will be analysed in detail in the next paragraph.

The mix design of the mortar's matrix proposed was obtained by using Portland cement 32.5R type II/B-LL with the inclusion of fine-grain sand and hydraulic lime, with the ratio 1/3+1/3+1/3 as most common, in central Italy, in the middle of the last century. The specimens have dimensions of 160x40x40 mm, and their seasoning was done for 28 days with constant temperature and humidity.

First, three-point bending tests were carried out, and a controlled displacement technique is used, i.e. a soft device was adopted, to detect the softening branch. The force-displacement curves obtained for each specimen are reported in Figure 3, where it is possible to observe a reduced softening branch in accordance with the expected tensile fragile behaviour of the mortar itself.

Note that with the beam theory we get $f_f = 3F_{max}L/(2s^2h)$ providing an estimate of the tensile (flexural) strength of the material, where L=160mm, h=s=40mm. The values are reported in Tab. 2, where the average strength is $f_{f,medium}$ = 3.45 MPa, which will be used for subsequent calibrations.

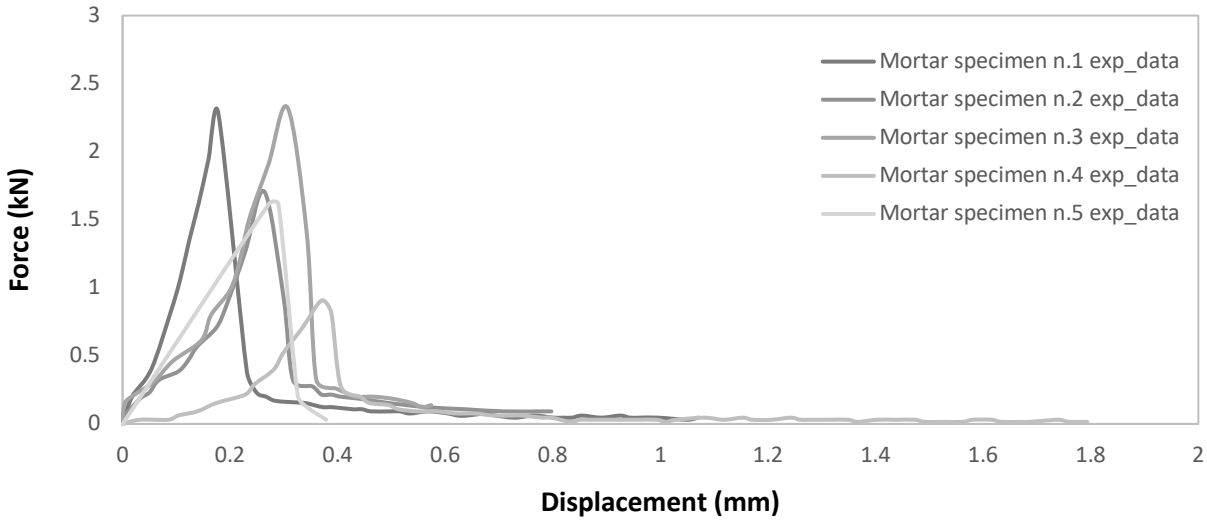

Figure 3 - Monotonic 3-point bending tests on the mortar specimens.

After the above-mentioned procedure, the two parts of the 3-point specimen were subjected to load-bearing tests to record the maximum compressive strength, also studying the softening behaviour. Obviously, all the specimens were previously regularized and capped, with average dimensions of 80x40x40mm. In Fig. 4, the force-displacement relationships are reported for all the specimens, confirming the reduced ductility of the mortar also in compression: once the maximum force is reached, the damage evolution is extremely rapid.

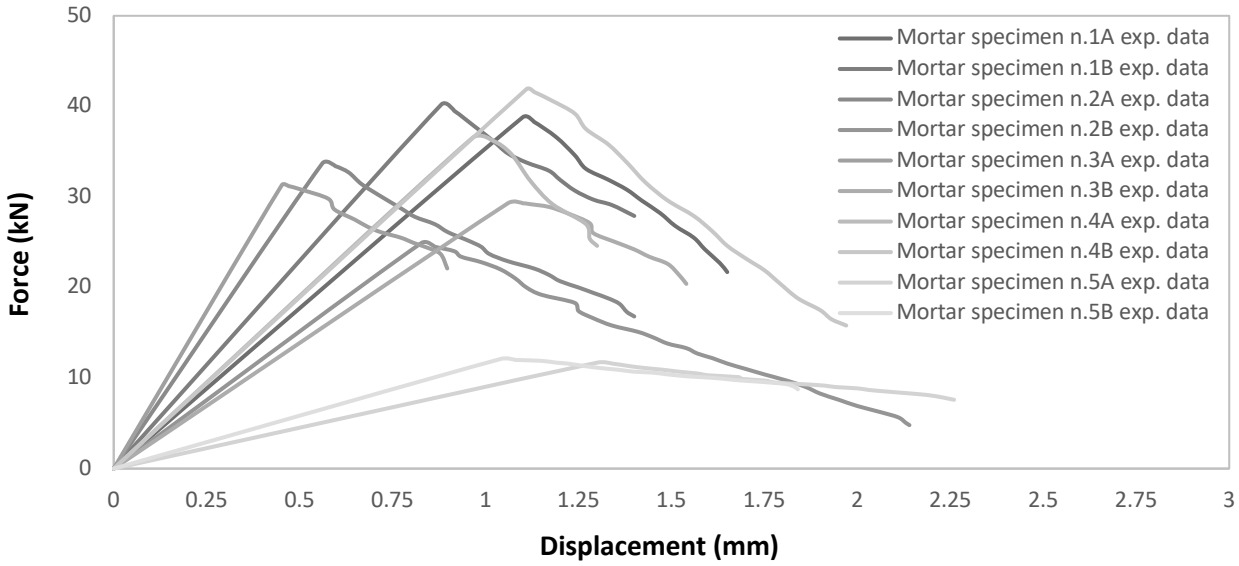

Figure 4 - Monotonic load-bearing tests on the mortar specimens.

For the mortar, a medium value 18.77 MPa of compressive resistance ($f_{c,medium}$) is evaluated, with an associate medium strain $\varepsilon_c(f_{c,m})$=1.16%, and an ultimate strain ε_u=2.06%, which will be used for subsequent calibrations.

Table 2 – Mortar specimens under 3-point bending and compression tests.

N.	$F_{flexural,max}$ (kN)	f_f (MPa)	$F_{c,max}$ (kN)	f_c (MPa)	ε_c (-)	ε_u (-)
Mortar spec. n.1A	2.28	5.34	38.8	24.25	1.4%	2.1%
Mortar spec. n.1B			40.2	25.13	1.1%	1.8%
Mortar spec. n.2A	1.71	4.01	33.7	21.06	0.7%	1.8%
Mortar spec. n.2B			24.9	15.56	1.0%	2.7%
Mortar spec. n.3A	2.32	5.44	31.3	19.56	0.6%	1.1%
Mortar spec. n.3B			29.3	18.31	1.3%	1.9%
Mortar spec. n.4A	0.91	2.13	36.5	22.81	1.2%	1.6%
Mortar spec. n.4B			41.9	26.19	1.4%	2.5%
Mortar spec. n.5A	1.61	3.79	11.7	7.31	1.6%	2.8%
Mortar spec. n.5B			12.1	7.56	1.3%	2.3%

4.3. Masonry specimens' setup

Four wall matrices with stones of different sizes and shapes, to reproduce as closely as possible the real walls shown in Figure 1, were constructed in a day inside the laboratory. In Figure 5 subsequent step of the wall matrix construction is reported. A double leaves technique was used with stones with a rougher surface, with sporadic wedges between stone layers, and the mortar placed to regularize the

horizontal layer from which to restart. The data lead to determine that the mortar had a non-constant thickness in the various layers as seen in the surveys carried out on structures built in the 1950s and 1960s, and this immediately leads ones to observe that it will play a crucial role in the response of the wall.

Two different tests were performed: a load-bearing test to establish the behaviour under vertical static loads for only a wall (Wall #4), and load bearing-shear tests in order to establish the resistance to horizontal actions acting in the panel plane for all three walls (Wall#1 to #3).

Table 3 - Wall specimens' geometries.

Wall	**Base (mm)**	**Length (mm)**	**Height (mm)**
#1	760	846	500
#2	750	862	500
#3	720	860	500
#4	740	857	500

The main dimensions of the masonry walls are reported in Tab. 3. Every wall rests on a 500x1200x15mm steel plate which is used to handle the specimen without damaging it up to the contrast frame. Identical plates are then positioned above each specimen to create a perfectly horizontal levelling and a load distribution plane. For the load-bearing-shear test, another plate was accounted to provide slip between the surfaces of the walls and the heads of the presses, so to significantly reduce scrolling problems that could occur if one only plate remained.

Figure 5 - "Scaglia Rossa" limestone wall matrices construction steps with the application of the double leaves' technique of the four wall matrices.

Figure 6 shows the typical test apparatus, where the load was applied using six hydraulic jacks (max. load 500 kN each), two in the horizontal and four in the vertical directions, all fixed to the reaction frame. Hydraulic jacks were connected to a hydraulic control unit with a pressure transducer, enabling the measurement of the applied force.

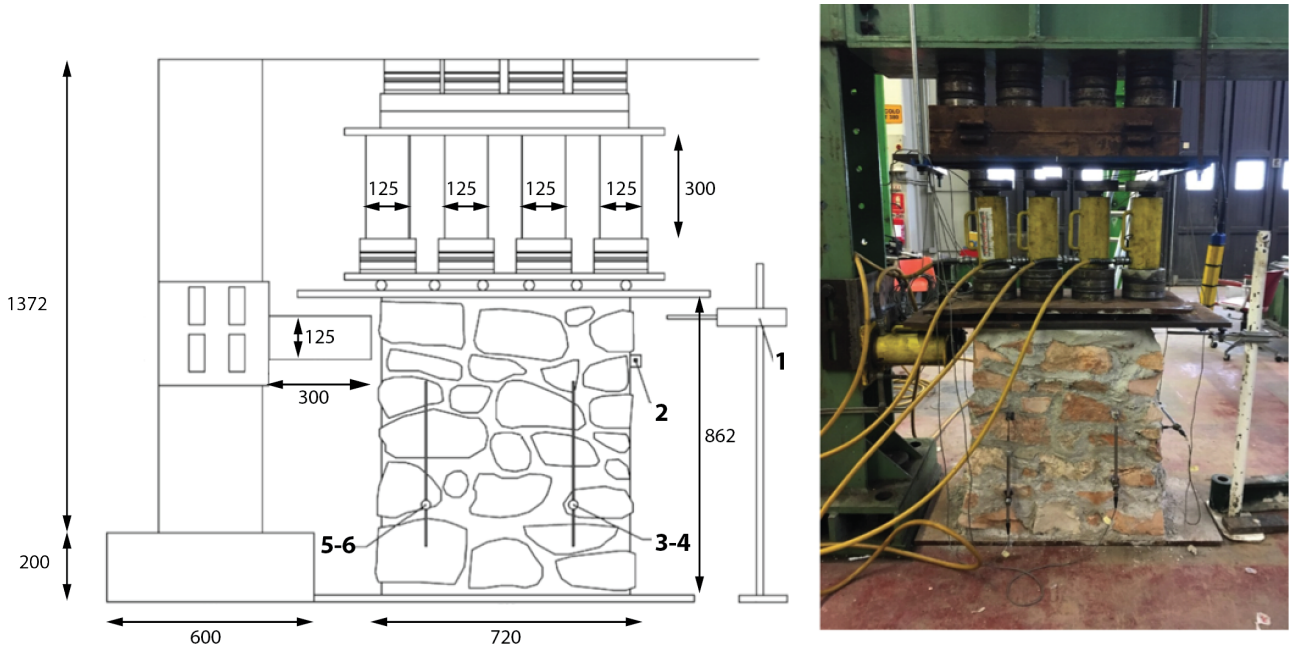

Figure 6 - Load bearing - shear apparatus with matrix specimen (measures in mm).

The specimen was enriched with transducers after its positioning in the apparatus, with a precision of 0.001 mm, in different points of the matrix. Four transducers (see Fig. 6) were used at the long faces of the specimen to obtain information on the compression and shearing loads (Numbers 3 – 6), one at the short right side of the specimen placed horizontally (Number 2), opposite to the heads of the hydraulic presses and the last one at the right short side of the specimen to measure the horizontal displacement of the wall in shearing (Number 1).

4.3.1 Load bearing test for the wall matrix

The load-bearing test for the wall matrix follows the Italian legislation, provided by UNI EN 1052-1:2001. The compression test aims to understand the level of axial force that can be supported by the

specimen and to provide useful indications in presence of only vertical forces. In this case, we merely used vertical hydraulic jacks, with a force-control system, which allow reaching a maximum force of almost 2000kN. In Figure 7, the force-displacement reported curve was obtained by using two LVDT between the frame and the steel plate at the top of the specimen to gain the displacement.

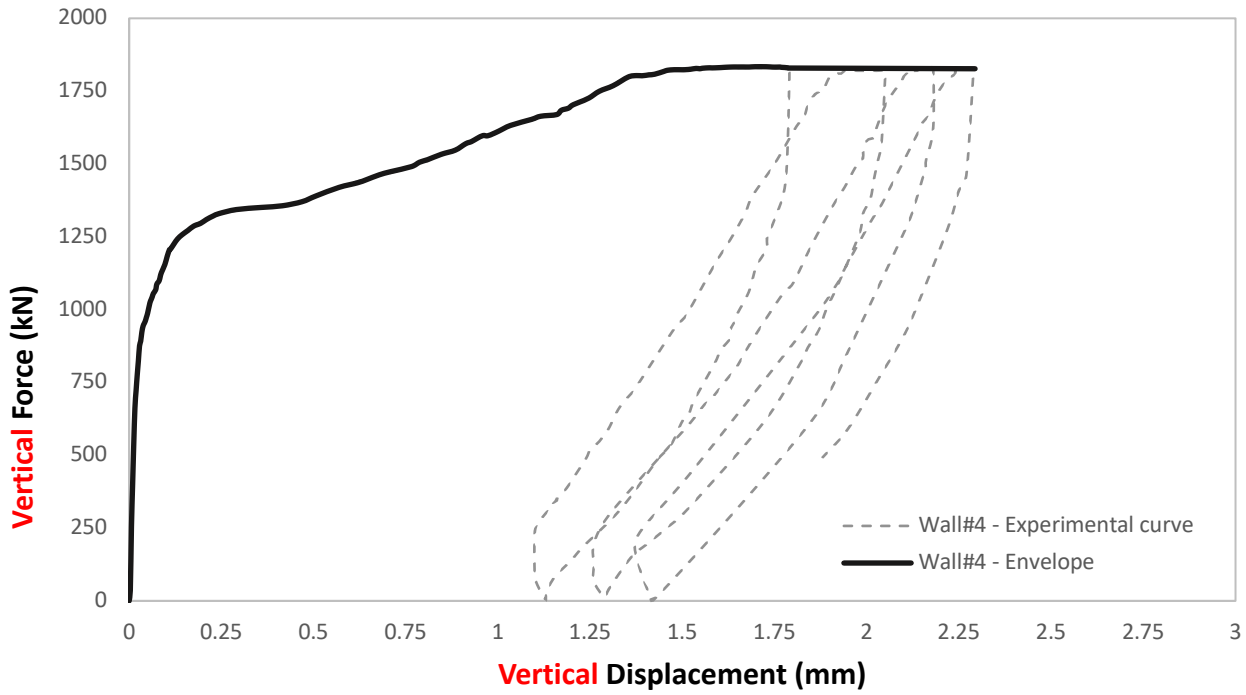

Figure 7 – Force - Displacement (kN - mm) diagram with envelope curve for Wall#4 subjected to load-bearing test.

(a) *(b)* *(c)*

Figure 8 - Wall matrix with displacement transducers installed (a), and the damage at the end of the compression test (b,c).

In the range of 800 kN the displacement values are almost zero, going further to 900÷1200 kN range, where the augmenting displacements are noticeable. The curve peak follows a trajectory up to the 1800 kN range where a clear plateau is visible (Fig. 7).

Once the plateau was reached, three sets of loading and unloading cycles were applied to evaluate both the residual displacement and the possible cumulated damage produced by the cycles. As can be seen from Fig. 7 and Fig. 8, the wall has reached its ultimate axial limit but can withstand further loading and unloading cycles without a clear decrease in stiffness.

Even if cracks were generated during this procedure, the compressive resistance of the wall matrix was calculated as $f_{c,w}=N_{max}/(B\cdot L) = 4.86$ N/mm^2.

4.3.2 Shear-compression test for the wall matrix

Figure 6 shows the sample set-up for shear-compression tests with a constant precompression load. The test configuration is the same as the axial compression tests. A precompression load of 400 kN, corresponding to a level axial load ratio $N/(Af_{c,w})\%=22\%$, was applied at the top end through four hydraulic jacks and kept constant throughout the whole test, to consider on the walls the presence of a vertical load of a typical floor. Afterwards, the two horizontal hydraulic actuators are activated once the stabilization for the vertical force has occurred.

The resulting shear force-displacement curves for the three specimens are reported in Figure 9.

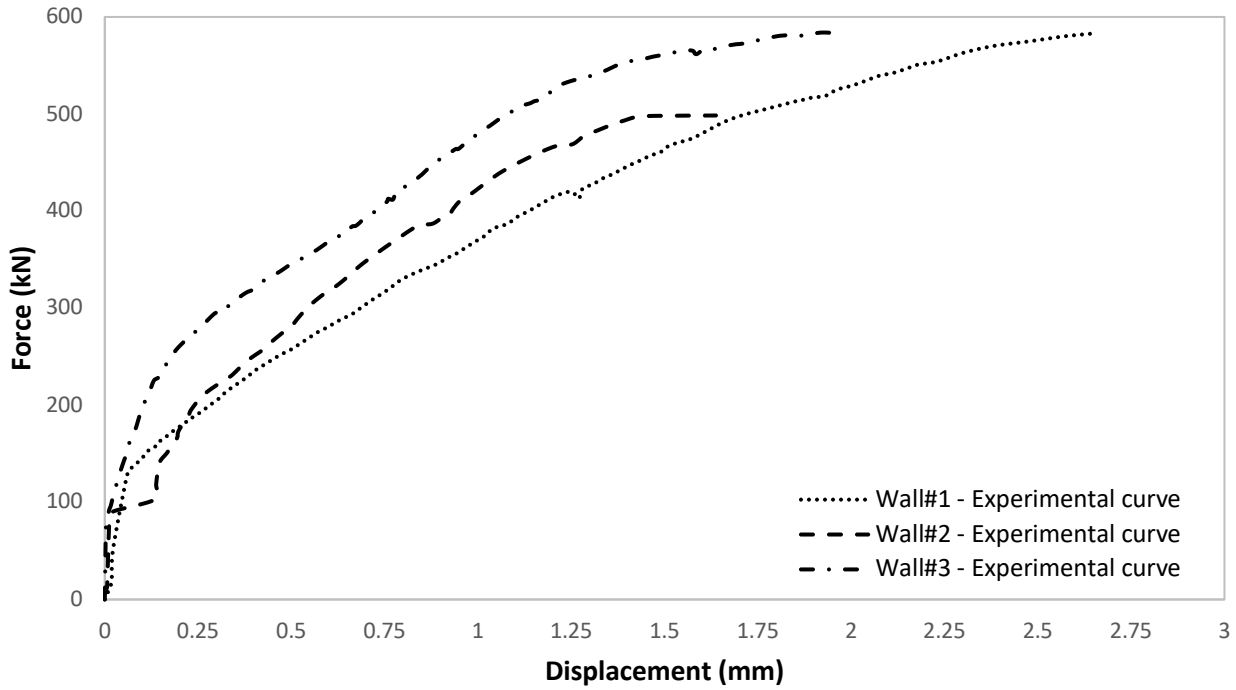

Figure 9 - Horizontal Force vs Displacement (kN - mm) diagram for Wall#1 to #3 subjected to shear test.

All the tests showed a homogeneous overall behaviour, with a maximum resistance that stood above 500 kN, except for local criticalities. Regarding Wall#1 the maximum force is 580 kN, reached when the displacement is over 2.6 mm, or alternatively when the drift is 0.31%. For Wall#2, the maximum force of 500 kN is attained when the drift is 0.18%, and for Wall#3 the maximum force of 580 kN is obtained for a drift of 0.22%. All the drift are comparable to those reported in Italian Standard [26,27] for nonlinear analysis of masonry's walls. Furthermore, it is possible to observe the absence of a plateau due to a highly fragile behaviour once the maximum force is reached. In fact, analysing the damage at the end of the test as reported in Fig. 10, the diagonal rupture due to compression and shearing deformations is always visible in all specimens. In some cases, panel disintegration was observed when the maximum force applied was reached.

(a) *(b)* *(c)*

Figure 10 - Damaged matrices at the end of the tests for Wall#1 (a), Wall#2 (b), Wall#3 (c).

This gives us a good representation of the non-monolithic behaviour of such matrix, which may be found commonly in stone walls made by substantially joined faces, with little diatones providing the transversal connection.

5. FEM ANALYSIS AND NUMERICAL RESULTS

Several Finite Element Models (FEMs) were developed to reproduce the data of the whole experimental campaign (axial compression tests in stone and mortar, and shear-compression tests with a constant precompression load in masonry). All the resistance parameters obtained from the single experimental tests, as reported in §4, are chosen to be fixed points of the subsequent numerical calibrations. Moreover, a tuning process was carried out to obtain other resistance parameters not deriving directly from the experimental tests, considering macro- and micro-modelling approaches.

For the numerical model definition, the open-source software Code Aster© was used; it is developed by EDF (Eletricité de France) [5]. The code has a wide variety of nonlinear material models in its library. The code is implemented in the Salome-Meca software, a mighty tool for open simulations.

To consider the non-linearity of the material, Mazars damage model was utilized. It is an isotropic scalar damage model, effective and easy to manage, which is limited by not taking into consideration the restoration of stiffness due to the closure of the crack's developed, and for this reason it is very

suitable for monotonous tests as those reported in the present work. The initial introduction and use of this damage constitutive model concerned the concrete. The calibration was performed by using the Levenberg - Marquardt algorithm, provided in the Code Aster© code; it is presented in the next sections along with the Mazars damage model.

5.1 Damage Model of Mazars

The Mazars damage model in its original formulation is a three-dimensional [28,29], isotropic model that leans on a criterion of damage written by strains and describes the dissymmetry between traction and compression. It has the advantage of requiring a reduced number of plainly physical parameters for its description.

The most common aim of damage mechanics is to describe and model the evolution of the degradation phenomena from a microscopic scale, starting from an undamaged initial or pre-stressed state, up to the creation of the damage (crack), known as the macroscopic scale.

8 parameters are required for the definition of the Mazars damage model. In addition to the elastic properties, Young's modulus E and Poisson's coefficient ν, the model facts of intervening 6 material's coefficients: A_c, B_c, A_t, B_t, k and E_0. Coefficients A_c, B_c, A_t and B_t allow to modulate the shape of the effective damage evolution law, the first two in compression and the other two in tension respectively, k is used to calibrate the asymptotic stress value at large displacement in shear and E_0 is the threshold of damage.

5.2. The Levenberg-Marquardt Method

The Levenberg – Marquardt algorithm (LMA) is an iterative technique that locates the minimum of a multivariate function F(x) that is expressed as the sum of squares of non-linear real-valued functions:

$$F(x) = \frac{1}{2}\sum_{i=1}^{m}[f_i(x)]^2 . \qquad (1)$$

Let the Jacobian of $f_i(x)$ be denoted $J_i(x)$, then the LMA searches in the direction given by the solution p to the equations $(J_k^T J_k + \lambda_k I)p_k = -J_k^T f_k$, where λ_k are non-negative scalars and I is the identity matrix. So, for some scalar Δ related to λ_k, the vector p_k is the solution of the constrained subproblem of minimizing $\|J_k\, p + f_k\|_2^2/2$ subject to $\|p\|_2 \leq \Delta$. It has now become a standard technique for non-linear least-squares problems, widely adopted in a broad spectrum of disciplines [30–34]. LMA can be thought of as a combination of steepest descent and the Gauss-Newton method. When the solution is far from the correct one, the algorithm changes its behavior and adopts the steepest descent method; slow but guaranteed to converge. When the current solution is close to the correct solution, it becomes a Gauss-Newton method.

In the literature there are other optimization methods, alternatives to LMA, and discussed here only for sake of completeness, such as a procedure based on a Genetic Algorithm (GA) [35] or a procedure based on the algorithm of Broyden – Fletcher – Goldfarb – Shanno (BFGSA) [36]. The GA is of stochastic nature and aims at the "survival" of the best solution through multiple attempts. The convergence of such an algorithm is defined by the creation of new individuals taken from an initial population that was created by a random process. The population each time progresses through the generations, evolves, and combines the best solution up until the point that a solution completely satisfies the criteria implemented and minimizes the objective function. The BFGSA, beginning from an initial guess defines the descent direction with a preconditioned gradient based on curvature information. It is an algorithm defined to solve unconstrained nonlinear optimization problems and remains less computationally complex when compared to Newton's method, [37–40].

In the current paper, the LGA was used to minimize the error between the data were taken by the experimental campaign and the numerical models in terms of Force – Displacement curves by perturbing the 8 parameters of the Mazars model, mentioned in Sect. 5.1, leaving the GA and BFGSA for further developments.

5.3 FEM for “Scaglia Rossa” stone

The experimental tests performed on the specimens of Scaglia stone (Tab. 1) showed the force necessary for the rupture of the specimens. Even if it was not possible to apply strain gauges to the surface of the specimens and receive the resulting force-displacement curves, a measurement of the specimens was done after the tests which showed a difference between the heights of the specimens in the range between 3 to 4 mm.

Considering the exact geometry of the cubic specimens reported in Table 1, the LGA was applied on FEMs to acquire numerically a measure for the elastic moduli. The FEMs were composed of 395 nodes and 1466 tetrahedral elements, and nonlinear behavior is used governed by the experimental value of $f_{c,s}$ reported in Table 1. The calibrations give us a medium value of the Young’s Modulus of the stones E_{stone}=16340 MPa, a value in good agreement with those found in the literature for limestones [41]. Finally, we want to stress the condition that, since the compressive force-displacement curve is not available for the stone, it was not possible to calibrate the Mazars’ model parameters. These values will be derived from the calibration of the micro-modeling approach, as reported in Sect. 5.5.2.

5.4 FEM for mortar

5.4.1 Three-point bending test

Prismatic numerical models for the 3-point bending tests of mortar shall be first considered. In this case, a displacement is applied in the middle and a reaction is measured considering the nonlinear response, to catch the softening branch.

Starting with the resistance parameters obtained from the single experimental tests, and synthesized in Table 2, the LMA is used for the calibration of the 8 Mazars' parameters. The optimized force-displacement (kN - mm) curves are reported in Fig. 11 with the dashed line and directly compared with the experimental ones reported with a continuous line. The loading part of the experimental data was not completely adjusted to the calibration process, but the peak values and the softening branch gave good fitting results.

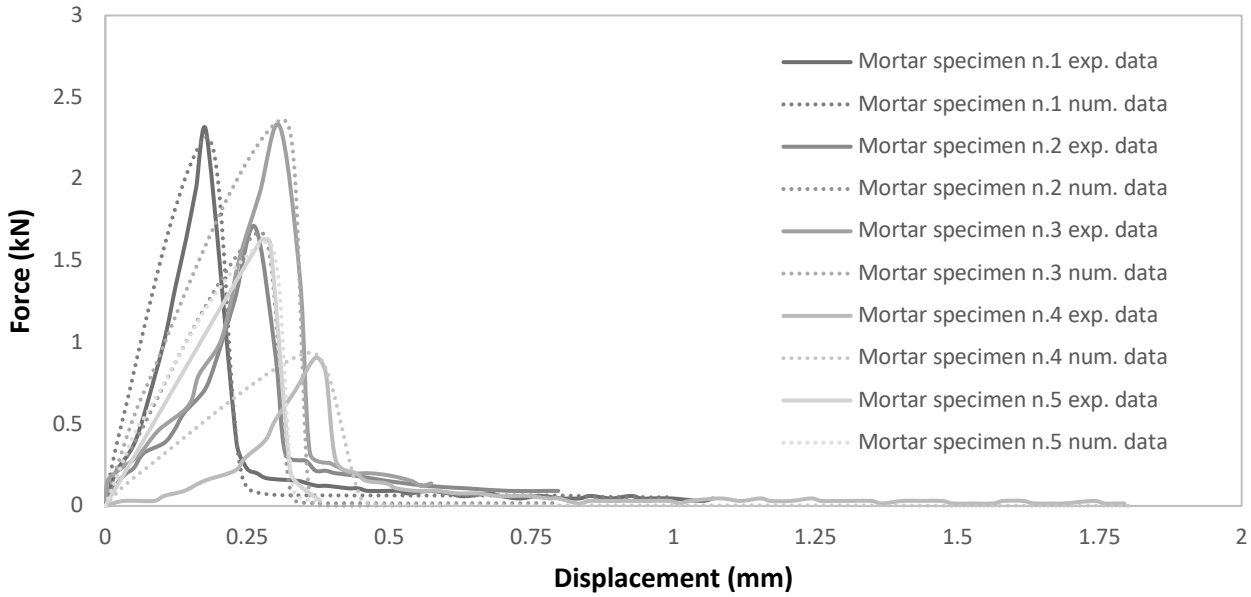

Figure 11 - Comparison between the experimental and numerical results from the optimization process with the Levenberg-Marquardt method for the 3-point bending test on mortar.

Table 4 - Optimizing Mazars' parameters (and relative error) obtained with the Levenberg - Marquardt algorithm for the 3-point bending test on mortar.

	E (MPa)	**ν**	**A_t**	**A_c**	**B_t**	**B_c**	**k**	**E_0 (10^{-5})**	**Error (%)**
Mortar spec. n.1	3000.0	0.10	0.18	2.00	5270	2530	0.804	1.51	6.22
Mortar spec. n.2	1300.0	0.108	1.00	2.00	9430	1200	0.501	1.21	13.40
Mortar spec. n.3	1750.0	0.122	1.00	2.00	3820	1270	0.501	0.10	15.19
Mortar spec. n.4	570.0	0.103	1.00	2.00	20600	709	0.50	1.71	15.13
Mortar spec. n.5	1206.5	0.186	0.99	2.00	9640	1070	0.692	30.70	0.43
Medium value	**1565.3**	**0.124**	**0.834**	**2.00**	**9752**	**1355**	**0.600**	**7.05**	-

In Table 4 are reported the calibrated values of coefficients of the Mazars' model for the 3-point bending test of mortar specimens. The medium value of the shape coefficients $A_{t,m}$=0.834 and $B_{t,m}$= 9752, and an equivalent strain at the beginning of the damage process $E_{0,m}=7.05\cdot10^{-5}$ confirm the absolutely fragile post-peak tensile behaviour.

5.4.2 Load-bearing tests

The numerical model for the load-bearing test was defined as a perfect prismatic three-dimensional element. In this case, the loading was performed by displacement control over the top side of the element. The number of nodes for these models is equal to 1396 and the number of tetrahedral elements is 5466.

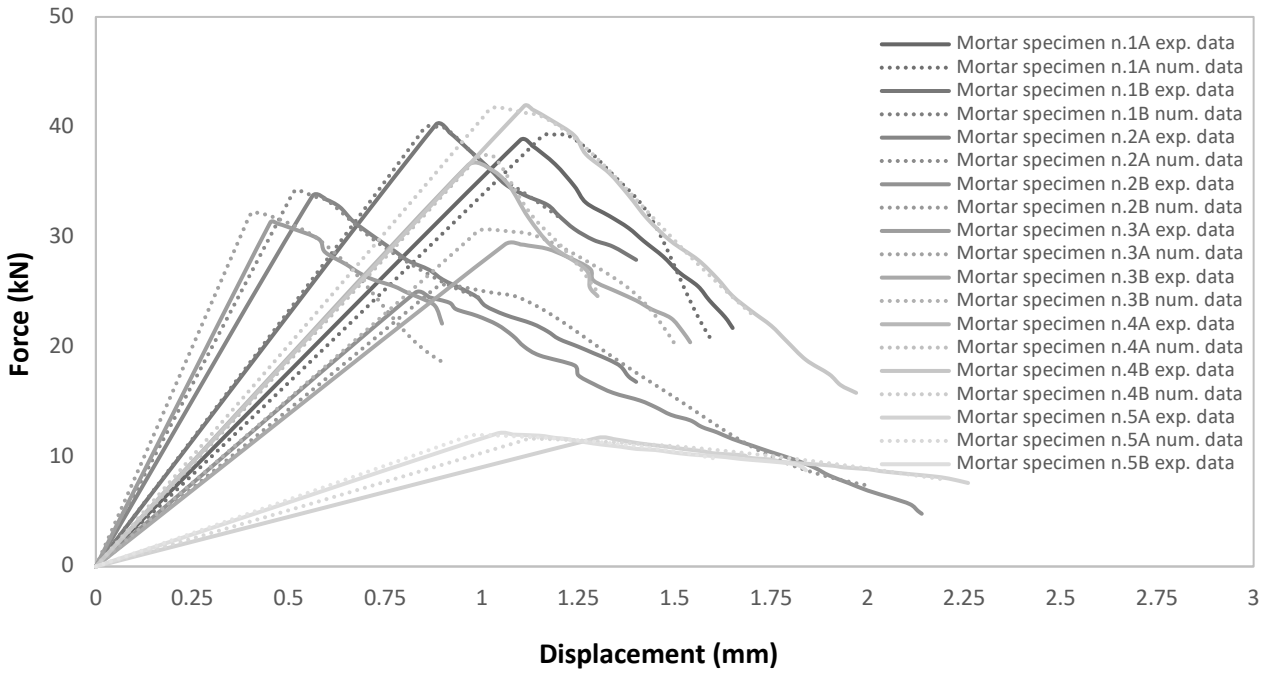

Figure 12 - Comparison between the experimental and numerical results from the optimization process with the Levenberg-Marquardt method for the load bearing test on mortar.

A close-fitting is obtained with the Levenberg - Marquardt algorithm as synthesized in Fig. 12 in terms of force-displacement curves, with a perfect fitting in both loading and unloading paths. The parameters that represent the evolution of Mazars damage model for the numerical specimens' optimization are presented in Table 5. A medium value of Young's module is 1895.19MPa, and a medium value for Poisson's coefficient of 0.226 are identifiable.

The resulting damage is concentrated in the middle of the specimens and follows a diagonal evolution until the end of the simulation. This rupture is associated with a medium value of the shape coefficients $A_{c,m}$=0.704 and $B_{c,m}$= 453.1, and an equivalent strain at the beginning of the damage process $E_{0,m}=3.69\cdot10^{-3}$, this last with two orders of magnitude higher than in the case of 3-point bending, confirming a less fragile post-peak behaviour in compression respect to the bending one.

Table 5 - Optimizing Mazars' parameters (and relative error) obtained with the Levenberg - Marquardt algorithm for the load-bearing tests on mortar.

N.	E (MPa)	ν	A_t	A_c	B_t	B_c	k	E_0 (10^{-3})	Error (%)
Mortar spec. n.1A	1653.24	0.162	0.617	0.900	8690	414	0.500	3.39	0.1176
Mortar spec. n.1B	2284.50	0.227	0.953	0.562	8790	500	0.653	3.50	0.0002
Mortar spec. n.2A	3268.11	0.223	0.854	0.526	8230	746	0.757	2.06	0.0007
Mortar spec. n.2B	1400.00	0.248	0.998	0.983	8990	300	0.698	4.00	0.4299
Mortar spec. n.3A	3957.07	0.184	0.279	0.608	1440	855	0.500	1.32	0.1381
Mortar spec. n.3B	1500.00	0.223	0.999	0.952	8990	293	0.699	4.00	0.0178
Mortar spec. n.4A	1836.13	0.203	1.500	0.588	10400	590	1.370	3.63	0.0038
Mortar spec. n.4B	1952.84	0.325	0.194	1.000	6860	208	0.500	6.09	0.0018
Mortar spec. n.5A	500.00	0.266	0.859	0.589	5630	222	0.525	5.42	0.0109
Mortar spec. n.5B	600.00	0.199	1.060	0.327	8810	403	0.762	3.49	0.0025
Medium value	**1895.19**	**0.226**	**0.831**	**0.704**	**7683.0**	**453.1**	**0.696**	**3.69**	**-**

5.5 FEM for masonry walls

This paragraph displays the calibration of the FEM of the masonry's panels with macro-and micro-modelling approaches (see Fig. 13), considering also the numerical results reported in §5.3 and §5.4.

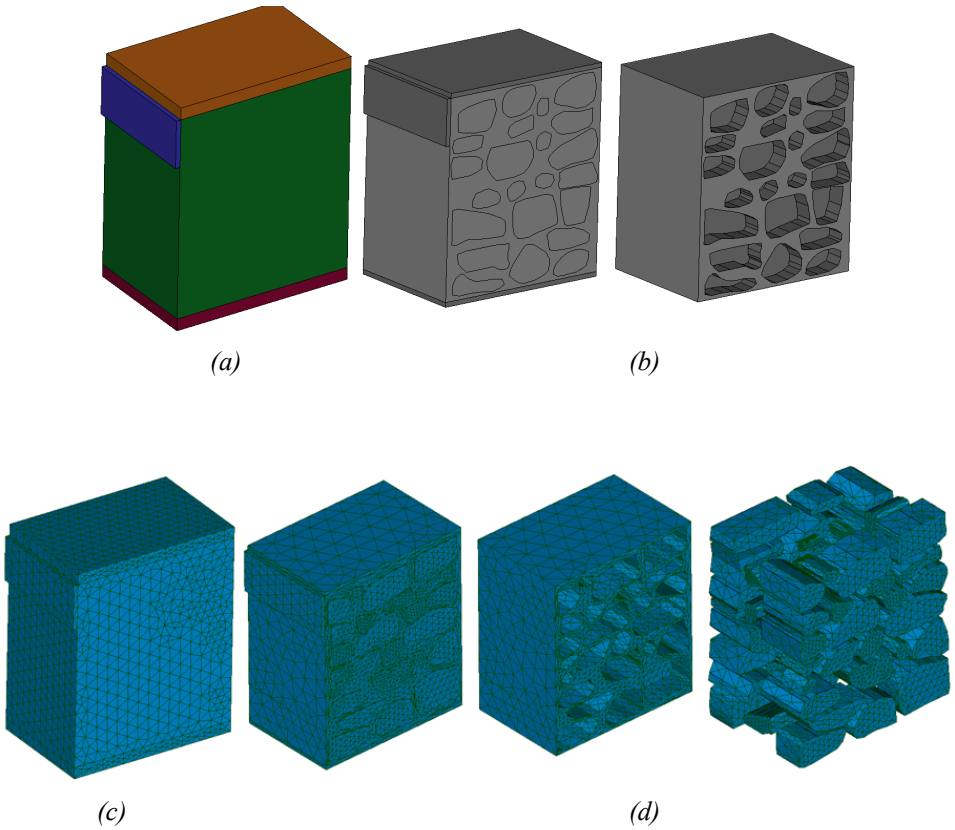

Figure 13 – Macro- (a,c), and micro- modelling (b,d) geometries and mesh representation with the presence of steel plates.

The geometry of the models reflects what is reported in Table 3 in terms of main dimensions, with a peculiar difference for the micro-modelling approach where the texture was reconstructed, with detail, following the survey carried out during the realization of the four walls as also visible from Fig. 5.

For the load-bearing (Wall#4) and the shear-compression tests' (Wall #1 to #3) simulations, the steel plates at the top, bottom and left side were also modelled to ensure a correct propagation of the forces, near the experimental ones.

5.5.1 Macro-modelling approach

The load-bearing-shear model was constituted by 3887 nodes and 16930 tetrahedral elements. In the case of the load-bearing model, the node number rises to 4231 while the number of tetrahedral elements descends to 16445. The left side panel takes the place of the two distinct pressure heads

with an equivalent plate. The decision to model this part was to reduce errors in the calculation by mesh incompatibility. The loading was given at the top and left face of the equivalent steel plates of the model while the bottom side of the model is fixed.

The force-displacement curves, obtained from the LM algorithm by changing the parameters of Mazars damage model and reported in Fig. 14, fit the experimental curves given in Fig. 9. It was possible in all cases to catch the whole progress of the compression-shearing process, with a minor discrepancy for Wall #2 and #3 caused by a progressive disaggregation of the masonry during the tests. The representation of the damage evolution was also coherent with the crack pattern obtained by the experimental tests as reported in Fig. 15.

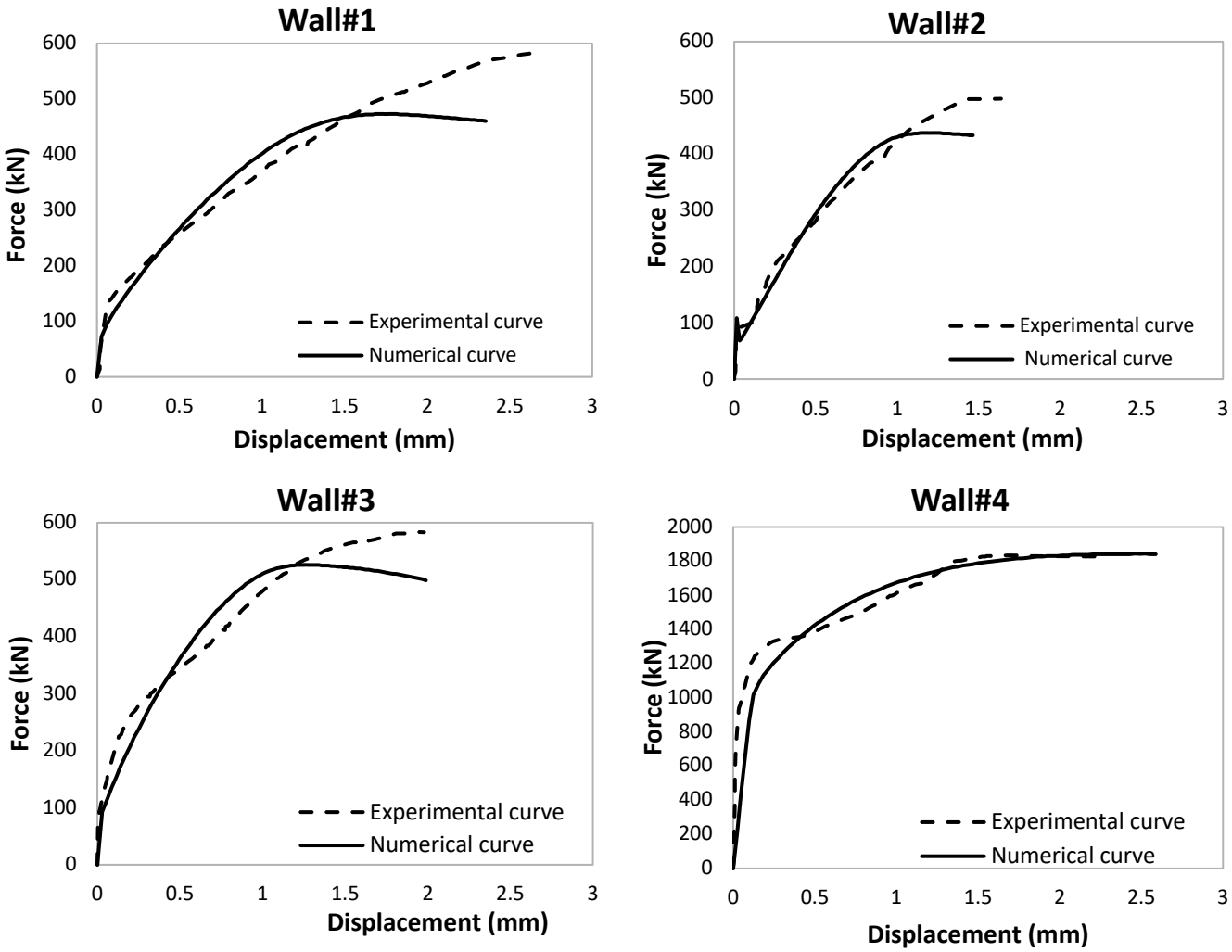

Figure 14 - Comparison between experimental and numerical force - displacement (kN - mm) curves after the calibration of the macro-modelling approach.

From Fig. 15, the damage presents itself in the upper-right and lower-left sides of the specimens where the model considers them immediately damaged (D = 1) and evolves around the middle part where the diagonal damage can be noticed (Fig. 15). This agrees with the experimental observation reported in Fig. 10, where damage is mainly concentrated on the diagonal and in the corner at the base.

The parameter's values that were obtained as results from the calibration process are finally represented in Tab. 5. For Wall #1, #2 and #3, an average Young's Modulus of 5517.57 MPa and an average Poisson's coefficient ν=0.14, and by Mazars Model a medium f_c=10.82 MPa and f_t=0.14 MPa are noticeable. Comparing these results with the values listed in Table C8.5.I of §C8.5.3 of [27], that the practitioners are obliged to use according to the requests of the Italian Standard NTC2018 [26], a comparison can be made with "Split stone masonry with good texture" for which E=1500÷1980 MPa, ν=0.5, and f_c= 2.6÷3.8 MPa. These values can be increased, with the presence of good mortar characterized by a medium compressive strength $f_{c,m}$, with a factor of $f_{c,m}^{0.35}$ in accordance with [27], providing final medium design values for E=4186÷5525 MPa, and f_c= 7.25÷10.6 MPa. A clear and important estimate is therefore available with this study starting from the tabulated data.

Table 5 - Optimizing Mazars' parameters (and relative error) obtained with the Levenberg - Marquardt algorithm with the macro modelling approach.

Wall	E (MPa)	ν	A_t	A_c	B_t	B_c	k	E_0 (10^{-5})	Error (%)
#1	6552.71	0.14	0.14	0.25	5000.00	200.00	0.66	0.11	3.44
#2	4000	0.23	0.73	0.42	6152.70	304.56	0.75	0.11	0.88
#3	6000	0.05	0.89	0.18	8310.00	528.59	0.53	0.10	4.34
Medium value of #1, #2, #3	**5517.57**	**0.14**	**0.58**	**0.28**	**6487.57**	**344.38**	**0.65**	**0.11**	-
#4	10000	0.40	2.50	0.10	18659.15	266.24	0.10	0.26	10.30

Finally, analysing the Mazars' parameters we can say that in compression the constitutive law comprising a parabolic hardening rule and a parabolic softening branch after the peak of resistance; the tension behaviour is better characterised by a linear hardening branch followed by a nonlinear softening branch with a remarkable brittle behaviour (see Tab. 5).

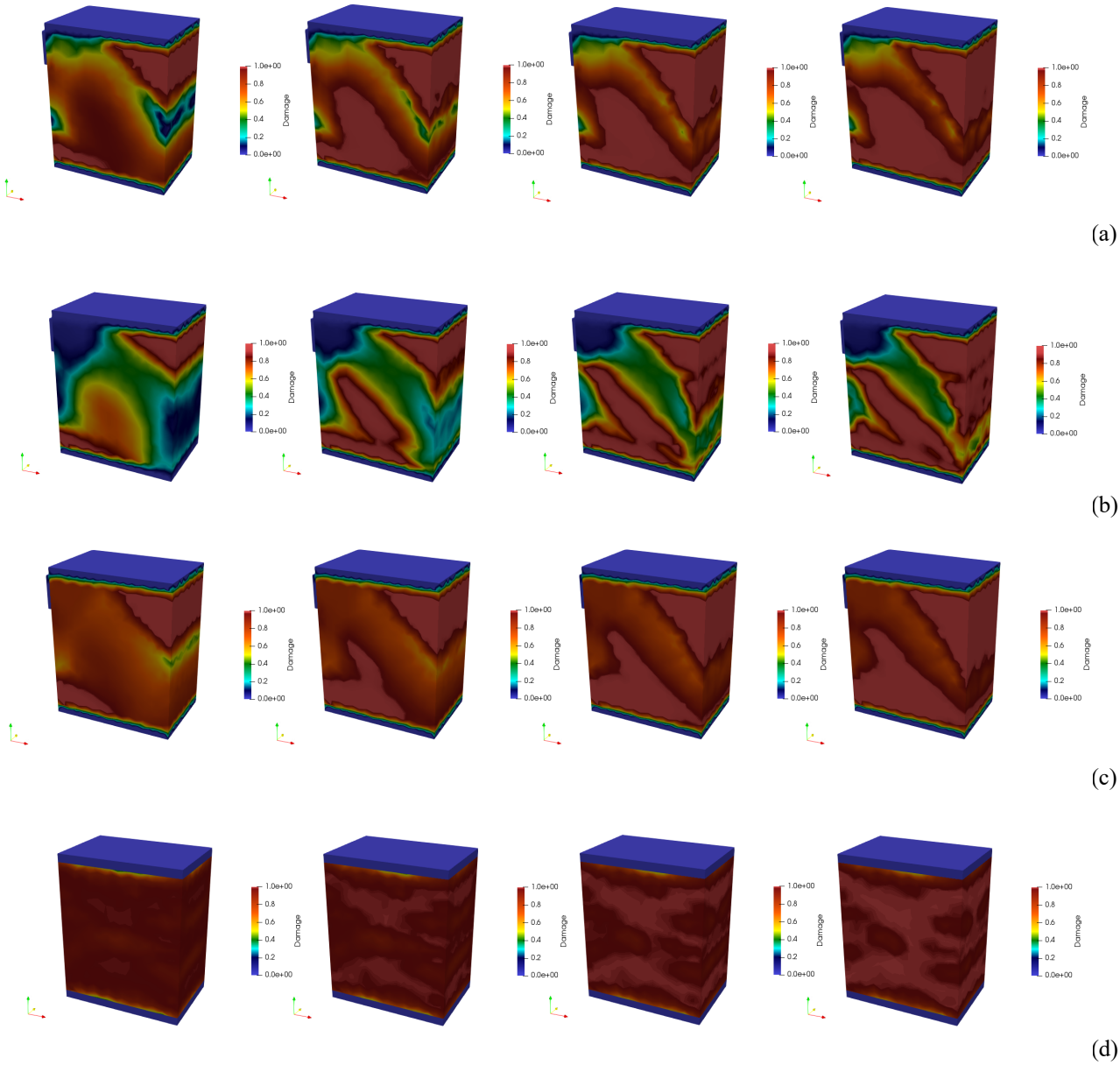

Figure 15 - Wall #1 (a), Wall #2 (b), Wall #3 (c) and Wall#4 (d) damage evolution for the 25%, 50%, 75% and 100% of the F_{max} (macro-modelling approach).

5.5.2 Micro-modelling approach

The simplified micro-modelling approach, a technique in which masonry units are represented as continuum elements interacting with the mortar joints, is considered as a reliable tool for the study of these experimental tests as it leads to distinguish with certainty the values of the mortar and the stones since it is an advanced tool for the numerical representation of the masonry. The purpose is to obtain more accurate results due to the possibility to consider different properties of joints and units, also simulating different failure mechanisms of masonry structures.

As far as the two different materials are concerned as starting Mazars' parameters values are considered the average values of the previous calibrations, with a scattering within the range established on the single element (see §5.3 and §5.4).

The results obtained by the procedure of optimization with the LM algorithm may be seen in Fig. 16, along with an accurate approximation of the numerical results in comparison to the experimental data.

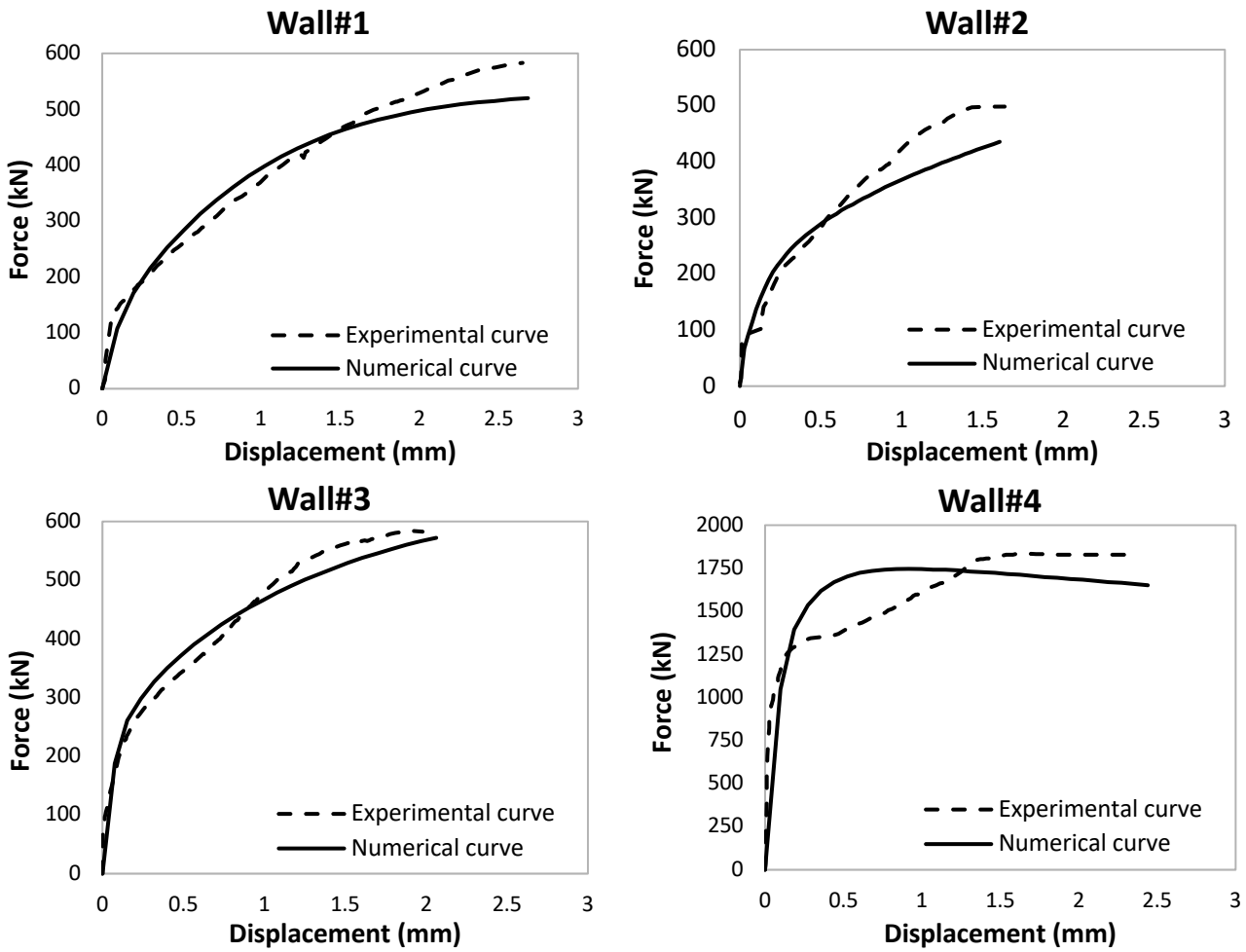

Figure 16 - Comparison between experimental and numerical force-displacement (kN - mm) curves after the calibration of the micro-modelling approach.

The parameters that the Levenberg - Marquardt algorithm provided as results are presented in Table 6 for stone, and in Table 7 for mortar. The main interest paraments, given the impossibility of a direct experimental quantification as already explained in §4.1, is Young's modulus of the stone, with and the average value of 18575.3 MPa, in good agreement with what has already been indicated in §5.3. All the Mazars' parameters confirm the fragile behaviour of the stone and mortar in tension, and a

very low equivalent strain at the beginning of the damage process $E_{0,medium} = 9.9 \cdot 10^{-6}$ which confirms, even more, the very fast activation of the structural damage.

Table 6 - Optimizing Mazars' parameters (and relative error) obtained with the Levenberg - Marquardt algorithm for the stone with the micro modelling approach.

Wall	E (MPa)	ν	A_t	A_c	B_t	B_c	k	E_0 (10^{-5})	Error (%)
#1	21000	0.25	1.05	0.93	6000	200	0.78	0.99	1.84
#2	18936.15	0.38	1.07	0.71	7532.17	200	0.76	1.00	2.79
#3	15789.75	0.29	0.51	0.59	11884.22	200	0.50	0.95	4.11
#4	17776.87	0.36	1.01	0.84	8889.21	413.15	0.71	0.99	12.52

Table 7 - Optimizing Mazars' parameters (and relative error) obtained with the Levenberg - Marquardt algorithm for the mortar with the micro modelling approach.

Wall	E (MPa)	ν	A_t	A_c	B_t	B_c	k	E_0 (10^{-5})	Error (%)
#1	4267.98	0.19	0.37	1.19	3020.65	200	0.50	0.96	1.84
#2	1139.65	0.17	0.87	0.32	7868.17	200	0.60	0.99	2.79
#3	4169.77	0.10	0.52	0.53	3967.60	200	0.51	0.93	4.11
#4	3577.12	0.32	0.18	0.10	11177.91	1681.25	0.85	1.11	12.52

In fact, the damage progression initially affects the mortar part of the model (D in the range of (0.6 - 1.0)) while presenting itself in some reduced part in the stone part of the model (D in the range (0.0 - 0.5). While the evolution is proceeding, the damage in the stone part of the model augments to different ranges (D in range the (0.6 - 1.0)) while the mortar part is already considered significantly damaged (Fig. 17). This behaviour was also seen in the experimental tests of the wall matrices in Sect. 4. In these cases, as opposed to the macro modelling, we cannot see clearly the diagonal damage, although we can assume the damage evolves in a diagonal pattern through the propagation. The assumption comes from the colour maps in Fig. 17: the upper right and bottom left corners are not affected while the intensity increased diagonally from the upper left to the bottom right corner, describing the expected diagonal propagation, confirming that seen with macro-modelling.

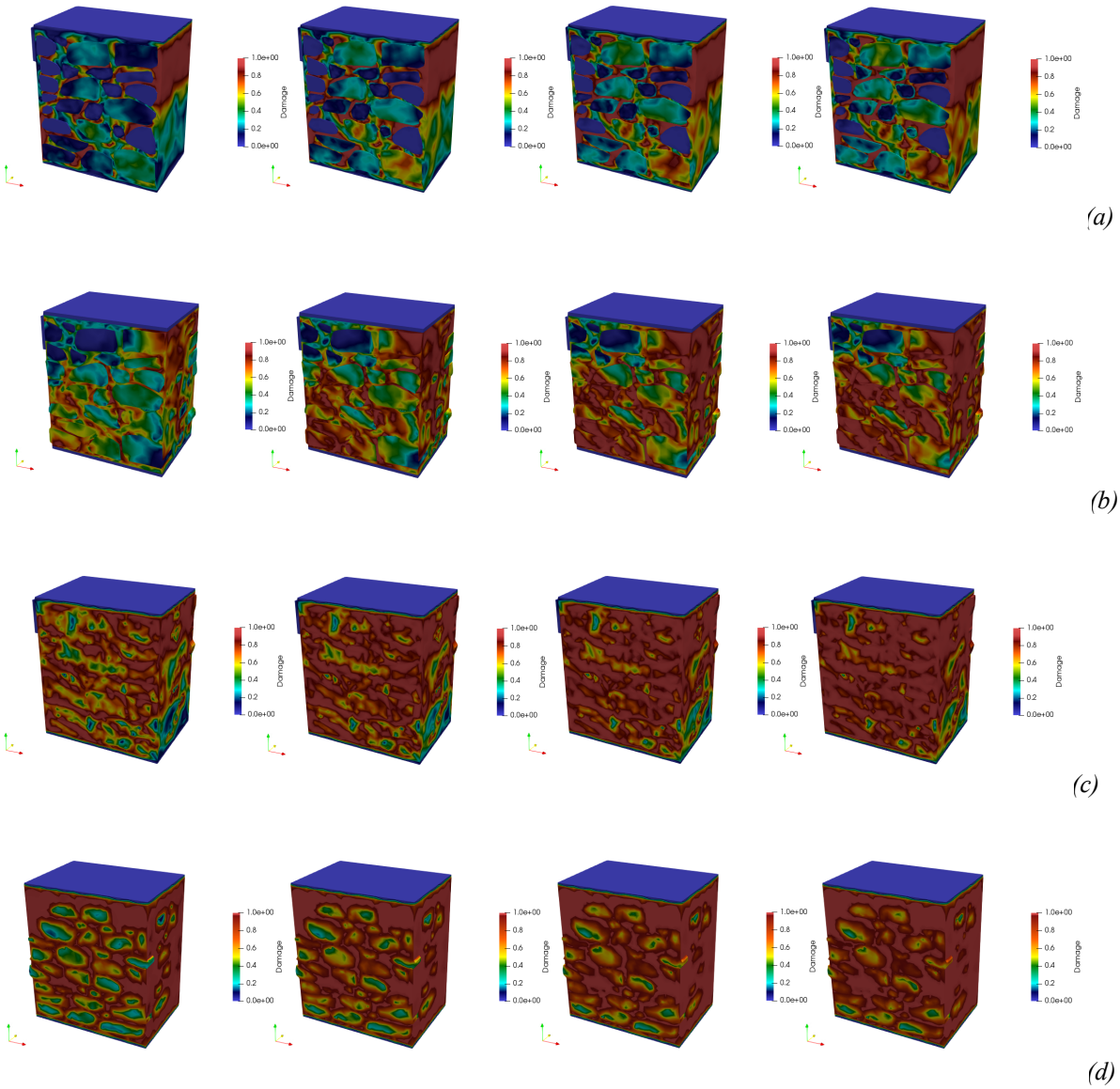

Figure 17 - Wall #1 (a) Wall #2 (b) Wall #3 (c) and Wall#4 (d) damage evolution for 25%, 50%, 75% and 100% of F_{max} (micro-modelling approach).

In the case of the simulation regarding the load-bearing test, it was noticed that the patterns generated between the two models are similar (Fig. 15(d) and 17(d)), although the micro-modelling approach gave better visual results of the damage evolution. As we may observe in the cases of micro-modelling, the damage evolution begins (D = 0) in the mortar part and propagates through the stone part of the model until complete damage is achieved (D= 1), confirming the damage reported in Fig. 10.

6. CONCLUSIONS

This paper outlines the studies carried on assessing the mechanical behaviour of masonry walls built by using the stone “Scaglia rossa”, a typical rock of the Apennine area between the Umbria and Marche Regions in Central Italy. Experimental tests and numerical analyses by FE method were performed to provide quantitative indications to all the professionals involved in the heavy reconstruction works that are now involving the area struck by the so-called Central Italy earthquake of 2016.

The experimental campaign involved several tests on the materials intending to characterize the constituent parts, stone and mortar, and the masonry assemblage reconstructed in the laboratory following the same techniques adopted in the 1950s-‘60s. Load bearing tests on “Scaglia Rossa” stone masonry underlined the wall’s capacity to reach its ultimate load and maintain a constant level of strength under further loading and unloading cycles, without a clear structural degradation. In presence of shear load, an evident fragile behavior connected with diagonal failure due to compression and shearing deformations was observed in all cases investigated; sometimes this was accompanied by the matrix disintegration. Several FE models were then developed to individually reproduce the data of the whole experimental campaign. Moreover, a calibration process was carried out by using the Levenberg - Marquardt algorithm to obtain. Results of numerical analyses obtained in terms of force-displacement curves and damage evolution have been compared with the experimental ones at varying of the modelling techniques.

With the macro-modelling technique, it was possible to obtain, starting from the experimental values, realistic values of the tensile and compressive strength of the "Scaglia Rossa" masonry. A more detailed analysis was then carried out which provided, based on the compressive strength of the mortar, a corrective parameter of the stiffness and strength of the "Split stone masonry with good texture" contained in the Italian Standard which allows to optimally fit the numerical stiffness and strengths obtained in the present work. Finally, all the Mazars’ parameters give us some ideas on the constitutive laws to use in the practice. In compression the constitutive law comprising a parabolic

hardening rule and a parabolic softening branch after the peak of resistance; in the tension behaviour the “Scaglia Rossa” masonry is better characterised by a linear hardening branch.

The micro-modelling technique gives a check on the value of Young's modulus of the stone which cannot be obtained from the experiments given the impossibility of instrumenting the very small stone’s specimens. Finally, the micro-modelling validates the enormous propensity to damage once resistance was tapped.

Declaration of Competing Interest

The authors declare that they have no known competing financial interests or personal relationships that could have appeared to influence the work reported in this paper.

Acknowledgement

The authors gratefully acknowledge the useful help provided by the technicians Andrea Conti and Franco Rinaldi.

References

[1] J.M. Jara, E.J. Hernández, B.A. Olmos, G. Martínez, Building damages during the September 19, 2017 earthquake in Mexico City and seismic retrofitting of existing first soft-story buildings, Eng. Struct. (2019) 109977. doi:10.1016/j.engstruct.2019.109977.

[2] K. Sharma, L. Deng, C.C. Noguez, Field investigation on the performance of building structures during the April 25, 2015, Gorkha earthquake in Nepal, Eng. Struct. 121 (2016) 61–74. doi:10.1016/j.engstruct.2016.04.043.

[3] M. Corradi, A. Borri, A. Vignoli, Strengthening techniques tested on masonry structures struck by the Umbria–Marche earthquake of 1997–1998, Constr. Build. Mater. 16 (2002) 229–239. doi:10.1016/S0950-0618(02)00014-4.

[4] D. Domínguez, F. López-Almansa, A. Benavent-Climent, Would RC wide-beam buildings in Spain have survived Lorca earthquake (11-05-2011)?, Eng. Struct. 108 (2016) 134–154. doi:10.1016/j.engstruct.2015.11.020.

[5] F. Clementi, A. Ferrante, E. Giordano, F. Dubois, S. Lenci, Damage assessment of ancient masonry churches stroked by the Central Italy earthquakes of 2016 by the non-smooth contact dynamics method, Bull. Earthq. Eng. 18 (2020) 455–486. doi:10.1007/s10518-019-00613-4.

[6] M. Corradi, A. Borri, A. Vignoli, Experimental study on the determination of strength of masonry walls, Constr. Build. Mater. 17 (2003) 325–337. doi:10.1016/S0950-0618(03)00007-2.

[7] L. Binda, A. Saisi, C. Tiraboschi, Investigation procedures for the diagnosis of historic masonries, Constr. Build. Mater. 14 (2000) 199–233. doi:10.1016/S0950-0618(00)00018-0.

[8] J.M. Pereira, A.A. Correia, P.B. Lourenço, In-plane behaviour of rubble stone masonry walls: Experimental, numerical and analytical approach, Constr. Build. Mater. (2020) 121548. doi:10.1016/j.conbuildmat.2020.121548.

[9] L. Berto, A. Saetta, R. Scotta, R. Vitaliani, An orthotropic damage model for masonry structures, Int. J. Numer. Methods Eng. 55 (2002) 127–157. doi:10.1002/nme.495.

[10] D. Liberatore, D. Addessi, Strength domains and return algorithm for the lumped plasticity equivalent frame model of masonry structures, Eng. Struct. 91 (2015) 167–181. doi:10.1016/j.engstruct.2015.02.030.

[11] D. Addessi, E. Sacco, A. Paolone, Cosserat model for periodic masonry deduced by nonlinear homogenization, Eur. J. Mech. A/Solids. 29 (2010) 724–737. doi:10.1016/j.euromechsol.2010.03.001.

[12] L. Gambarotta, S. Lagomarsino, Damage models for the seismic response of brick masonry shear walls. Part II: the continuum model and its applications, Earthq. Eng. Struct. Dyn. 26 (1997) 441–462. doi:10.1002/(SICI)1096-9845(199704)26:4<441::AID-EQE651>3.0.CO;2-0.

[13] L. Gambarotta, S. Lagomarsino, Damage models for the seismic response of brick masonry shear walls. Part I: the mortar joint model and its applications, Earthq. Eng. Struct. Dyn. 26 (1997) 423–439. doi:10.1002/(SICI)1096-9845(199704)26:4<423::AID-EQE650>3.0.CO;2-#.

[14] G. Janszen, P.G. Nettuno, Implementation and validation of a strain rate dependent model for carbon foam, in: Int. J. Mech. Sci., Elsevier, 2009: pp. 105–115. doi:10.2495/CMEM090101.

[15] S. Marfia, E. Sacco, Multiscale damage contact-friction model for periodic masonry walls, Comput. Methods Appl. Mech. Eng. 205–208 (2012) 189–203. doi:10.1016/j.cma.2010.12.024.

[16] R. Luciano, E. Sacco, A damage model for masonry structures, Eur. J. Mech. - A/Solids. 17 (1998) 285–303. doi:10.1016/S0997-7538(98)80087-9.

[17] A. Drougkas, P. Roca, C. Molins, Nonlinear micro-mechanical analysis of masonry periodic unit cells, Int. J. Solids Struct. 80 (2016) 193–211. doi:10.1016/j.ijsolstr.2015.11.004.

[18] F. Clementi, E. Quagliarini, G. Maracchini, S. Lenci, Post-World War II Italian school buildings: typical and specific seismic vulnerabilities, J. Build. Eng. 4 (2015) 152–166. doi:10.1016/j.jobe.2015.09.008.

[19] L. Sorrentino, S. Cattari, F. da Porto, G. Magenes, A. Penna, Seismic behaviour of ordinary masonry buildings during the 2016 central Italy earthquakes, Bull. Earthq. Eng. 17 (2019) 5583–5607. doi:10.1007/s10518-018-0370-4.

[20] C. Clementi, F. Clementi, S. Lenci, Nonlinear analyses and failure patterns of typical masonry school buildings in the epicentral zone of the 2016 Italian earthquakes, in: AIP Conf. Proc., 2017: p. 090005. doi:10.1063/1.5012362.

[21] A. Arêde, C. Almeida, C. Costa, A. Costa, In-situ and lab tests for mechanical characterization of stone masonry historical structures, Constr. Build. Mater. 220 (2019) 503–515. doi:10.1016/j.conbuildmat.2019.06.039.

[22] G. Vasconcelos, P.B. Lourenço, Experimental characterization of stone masonry in shear and compression, Constr. Build. Mater. 23 (2009) 3337–3345. doi:10.1016/j.conbuildmat.2009.06.045.

[23] J. Segura, L. Pelà, P. Roca, Monotonic and cyclic testing of clay brick and lime mortar masonry in compression, Constr. Build. Mater. 193 (2018) 453–466. doi:10.1016/j.conbuildmat.2018.10.198.

[24] P.B. Lourenço, Computational strategies for masonry structures : multi-scale modeling, dynamics, engineering applications and other challenges, Congr. Métodos Numéricos En Ing. (2013) 1–17. http://repositorium.sdum.uminho.pt/handle/1822/26547.

[25] A. Tomassini, Pietra Cesana - Tradizione autentica (in italian), (2021). https://www.pietracesana.it/materiale/.

[26] Ministero delle Infrastrutture e dei Trasporti, DM 17/01/2018 - Aggiornamento delle “Norme Tecniche per le Costruzioni” (in italian), (2018) 1–198.

[27] Ministero delle infrastrutture e dei trasporti, Circolare 21 gennaio 2019 n. 7 C.S.LL.PP. Istruzioni per l’applicazione dell’aggiornamento delle “Norme Tecniche per le Costruzioni” di cui al D.M. 17/01/2018 (in Italian), Suppl. Ord. Alla G.U. n. 35 Del 11/2/19. (2019).

[28] J. Mazars, A description of micro- and macroscale damage of concrete structures, Eng. Fract.

Mech. 25 (1986) 729–737. doi:10.1016/0013-7944(86)90036-6.

[29] J. Mazars, G. Pijaudier-Cabot, Continuum Damage Theory—Application to Concrete, J. Eng. Mech. 115 (1989) 345–365. doi:10.1061/(ASCE)0733-9399(1989)115:2(345).

[30] P. Roca, M. Cervera, G. Gariup, L. Pela', Structural Analysis of Masonry Historical Constructions. Classical and Advanced Approaches, Arch. Comput. Methods Eng. 17 (2010) 299–325. doi:10.1007/s11831-010-9046-1.

[31] K. Lin, H. Liu, C. Wei, Q. Huang, Effects of shear rate on cyclic behavior of dry stack masonry joint, Constr. Build. Mater. 157 (2017) 809–817. doi:10.1016/j.conbuildmat.2017.09.062.

[32] R. Morbiducci, Nonlinear parameter identification of models for masonry, Int. J. Solids Struct. 40 (2003) 4071–4090. doi:10.1016/S0020-7683(03)00170-7.

[33] M. Mishra, Machine learning techniques for structural health monitoring of heritage buildings: A state-of-the-art review and case studies, J. Cult. Herit. 47 (2021) 227–245. doi:10.1016/j.culher.2020.09.005.

[34] F. Khosravikia, J. Kurkowski, P. Clayton, Fragility of masonry veneers to human-induced Central U.S. earthquakes using neural network models, J. Build. Eng. 28 (2020) 101100. doi:10.1016/j.jobe.2019.101100.

[35] F. Bianconi, G.P. Salachoris, F. Clementi, S. Lenci, A Genetic Algorithm Procedure for the Automatic Updating of FEM Based on Ambient Vibration Tests, Sensors. 20 (2020) 3315. doi:10.3390/s20113315.

[36] R. Fletcher, Practical Methods of Optimization, John Wiley & Sons, Ltd, Chichester, West Sussex England, 2000. doi:10.1002/9781118723203.

[37] F. Mohammadi, B. Bina, H. Karimi, S. Rahimi, Z. Yavari, Modeling and sensitivity analysis of the alkylphenols removal via moving bed biofilm reactor using artificial neural networks: Comparison of levenberg marquardt and particle swarm optimization training algorithms, Biochem. Eng. J. 161 (2020) 107685. doi:10.1016/j.bej.2020.107685.

[38] H. Marouani, K. Hergli, H. Dhahri, Y. Fouad, Implementation and Identification of Preisach

Parameters: Comparison Between Genetic Algorithm, Particle Swarm Optimization, and Levenberg–Marquardt Algorithm, Arab. J. Sci. Eng. 44 (2019) 6941–6949. doi:10.1007/s13369-019-03727-8.

[39] B.M. Ozyildirim, M. Kiran, Do optimization methods in deep learning applications matter?, ArXiv. (2020).

[40] I. Mukherjee, S. Routroy, Comparing the performance of neural networks developed by using Levenberg-Marquardt and Quasi-Newton with the gradient descent algorithm for modelling a multiple response grinding process, Expert Syst. Appl. 39 (2012) 2397–2407. doi:10.1016/j.eswa.2011.08.087.

[41] Y. Zhang, F. Huang, Mechanism of different coseismic water-level changes in wells with similar epicentral distances of intermediate field, Bull. Seismol. Soc. Am. (2011). doi:10.1785/0120100104.